Dalton Transactions

Accepted Manuscript

ROYAL SOCIETY OF CHEMISTRY

www.rsc.org/dalton

Dalton Transactions

PAPER

Exploration of the mechanical behavior of Metal Organic Frameworks UiO-66(Zr) and MIL-125(Ti) and their NH_2 functionalized versions

Received 00th January 20xx,
Accepted 00th January 20xx

DOI: 10.1039/x0xx00000x

www.rsc.org/

Pascal. G. Yot,[*a] Ke Yang,[a] Florence Ragon,[b] Vladimir Dmitriev,[c] Thomas Devic,[d] Patricia Horcajada,[d] Christian Serre,[d] Guillaume Maurin,[a]

The structural behaviour under mechanical stimuli of two Metal Organic Frameworks, UiO-66(Zr) and MIL-125(Ti) and their amino-functionalized derivatives has been investigated by high-pressure powder X-ray diffraction up to 3.5 GPa. All these solids showed a gradual pressure-induced reversible decrease of their crystallinity and UiO-66(Zr)_NH_2 material was revealed as one of the most resilient MOFs reported so far orresponding to a very high bulk modulus. The mechanical behaviors of these MOFs have been correlated to their chemical and geometric features including the metal-oxygen coordination number, the nature of the organic linker, the porosity as well as their crystal density.

Introduction

Metal Organic Framework (MOF) materials have been the focus of intense research over the past 10 years, with the emergence of more than 20,000 architectures, constructed from the assembly of a large diversity of both inorganic units (clusters, chains) and organic moieties. Some of these hybrid porous solids have shown performances that sometimes surpass that of the conventional porous materials commercially used in diverse areas including storage of strategic gases, separation of fluids, catalysis, etc… [01, 02] A significant effort has been devoted since the last few years to characterize the water stability of these materials considered as one of the major drawbacks that would limit their uses for many applications. [3, 4] Their mechanical stability has received much lesser attention, [5-9] although this feature is of outmost importance since the MOFs are required to retain their crystallinity and porosity during both their shaping (pellets, membranes) and the different types of compression in play in the targeted applications.

Amongst the large number of MOFs reported so far, the UiO-66(Zr) (UiO stands for University of Oslo), the MIL-125(Ti) (MIL stands for Materials of Institut Lavoisier) and their amino derivatives [10-12] have shown promising performances in different fields including gas storage/separation, electro/photo-catalysis and optical response. [13-16], Interestingly, both families of materials have been demonstrated to possess good thermal and chemical stabilities that make them very attractive for further applications. Indeed they maintain their structure unaltered up to 600 K in air, and they are stable not only under moisture but also in the presence of contaminants such as H_2S. [16] This unique combination of stabilities is a clear-cut advantage compared to the majority of Cu-, Fe- and Zn- based MOFs reported so far. [17] The mechanical behaviour of the UiO-66(Zr) and the MIL-125(Ti) has been only scarcely explored so far. [18, 19] Beyond an interest from an application standpoint, the fundamental knowledge of the impact of both the framework topology and crystal density, the metal-oxygen and metal-organic coordination of MOFs and the functionalization of the organic linker on their mechanical properties is appealing. In this context, the selection of these 3D cages-type Zr- and Ti- based MOFs is relevant since these solids showing the same topology (i) are built from distinct structure building units (SBUs), i.e. cyclic octamers of edge- and corner-sharing $TiO_5(OH)$ octahedra for MIL-125(Ti)s and inner $Zr_6O_4(OH)_4$ cluster in which the triangular faces of the Zr_6-octahedron are alternatively capped by μ_3-O and μ_3-OH groups for UiO-66(Zr)s, (ii) the coordination of the metal center differs, the Ti atoms being six-coordinated, while the Zr atoms are eight-coordinated and (iii) their crystal density significantly differs (see Table 1).

Herein, the pressure-induced structural behaviour of these MOF materials under applied pressure up to 3.5 GPa is explored by means of high pressure powder X-ray diffraction (PXRP) with the objective to reveal (i) their pressure-domain stability, (ii) the evolution of their crystallinity and (iii) their compressibility via the determination of their bulk modulus. These whole data are further discussed in light of the framework topology, the metal-oxygen coordination and the functionalization of the organic linker of these MOFs. Finally these mechanical properties are compared to that reported so far in the literature for other rigid MOFs.

Materials and Methods

Materials

[a] Institut Charles Gerhardt Montpellier UMR 5253 CNRS UM ENSCM, Université de Montpellier, CC 15005, Place Eugène Bataillon, F-34095 Montpellier cedex 05, France. e-mail: pascal.yot@umontpellier.fr; Tel.: +33 4 67 14 32 94; Fax: +33 4 67 14 42 90.
[b] Institut Lavoisier Versailles, Université de Versailles St-Quentin, 45, avenue des Etats-Unis, F-78035 Versailles cedex, France.
[c] Swiss Norvegian Beamlines, European Synchrotron Radiation Facility, 3800 Grenoble, France.

Electronic Supplementary Information (ESI) available: Experimental procedures, X-ray diffraction, and molecular simulation. See DOI: 10.1039/x0xx00000x

The four samples were synthesized and characterized according to previously published procedures. [20-22]

More details about the synthesis procedures are given in the Electronic Supporting Information. Since this Zr-based MOF is known to show defects in the form of missing linkers,[23-27] Thermo gravimetric analysis (ESI, Fig. S1) [23] were performed to estimate their concentration in both UiO-66(Zr) and UiO-66(Zr)_NH_2. It was evidenced that these solids contain only a small concentration of missing linkers, i.e. 1 out of 12 total in the Zr-O coordination sphere. Such an identical number of defects for the two solids make the comparison of their mechanical properties fully consistent without the need in this study to explore the impact of the structural defects.

Powder X-ray diffraction

High pressure powder X-ray diffraction (PXRD) experiments were carried out at the European Synchrotron Radiation Facility on the Swiss Norvegian Beamline BM01A. All XRPD patterns were recorded at room temperature in a pressure range [10^{-4}–3.5 GPa] using a diamond anvil cell (DAC) with a wavelength λ=0.694120 Å. This strategy has been already used to characterize the structural behaviour of MOFs under applied pressure. [24,28-44] For each patterns the pressure was determined from the shift of the ruby R1 fluorescence line. Aldrich AP100 Silicone oil was used as a pressure-transmitting medium to give quasi-hydrostatic conditions since its kinetic diameter largely exceeds the window size of both porous solids which ensures that it does not enter into the pore. Profile analysis (Le Bail intensity fitting with refinement of lattice parameters) of individual powder X-ray patterns was performed using Jana 2006 software. [45]

Results

The resulting PXRD patterns for both UiO-66(Zr) and UiO-66(Zr)-NH2 are reported in Figures 1a and 1b. The Bragg peaks are only slightly shifted towards high angles in the whole range of applied pressure. All the recorded patterns are successfully indexed in the space group $F\bar{4}3m$ (See ESI fig. S2 and S3). The resulting evolutions of the unit cell parameters as a function of the applied pressure are plotted in Figure 2. Both solids show a gradual decrease of their unit cell volumes at the initial stage of the applied pressure up to 1 GPa followed by a step change that occurs in the pressure range 1.0-1.5 GPa. In contrast to our previous reported results for the MIL-53(Cr, Al) and MIL-47(V) series, these solids do not undergo any structural transition. The UiO-66(Zr) frameworks exhibit a relatively rigid character as illustrated by their unit cell volume variations lower than 10% at 3.5 GPa (see ESI). This observation confirms what has been previously reported by Guillerm *et al.* [18] for UiO-66(Zr) under an increasing uniaxial compression created by an Infra-red press up to 1 GPa. The mechanical stability of these solids comes from the high Zr-O coordination (8) and the high inorganic node-organic linker coordination (12) both parameters contributing to drastically enhance the resilience of such an architecture. These experimental findings are also consistent with the conclusions drawn by previous DFT calculations on UiO-66(Zr) that stated that such a structure undergoes only tiny changes under compression with a small shortening of the Zr-O distances as well as the distances between bridging bonds between the carbon atoms of the carboxylate group and the carbon of the phenyl rings. [19]

Both solids exhibit however a significant broadening of the Bragg peaks under increasing applied pressure (Figure 1). This is associated with a pronounced loss of crystallinity at moderate pressures that was evaluated using the Scherrer equation applied to the diffraction peak corresponding to the (111) plane (see ESI). The evolution of the normalized crystallinity in the whole range of pressure is reported for both UiO-66(Zr)s in Figure 3.

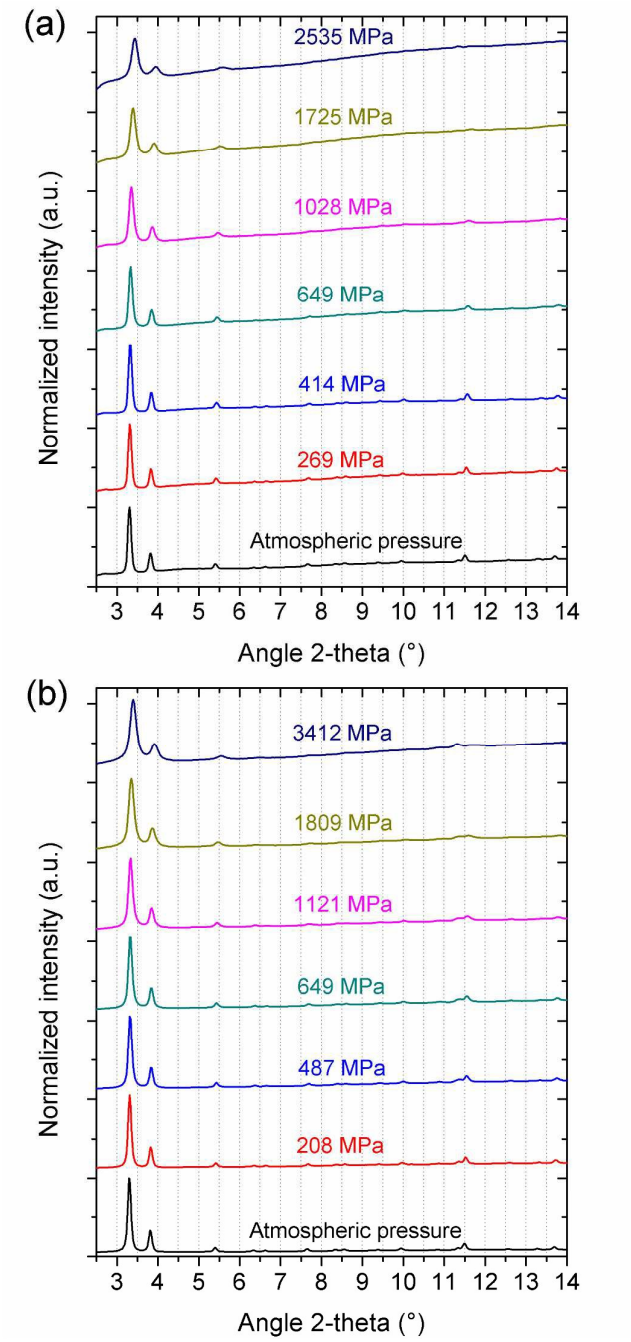

Fig. 1 *Powder X-ray diffraction patterns (λ= 0.694120 Å) obtained for the (a) UiO-66(Zr) and (b) UiO-66(Zr)_NH_2 as a function of the applied pressure at room temperature.*

These plots show a step-change at ~1.4 GPa and ~1.8 GPa for UiO-66(Zr) and its amino form respectively, followed by a smoother decreasing profile at higher pressure. This coincides well with the step-change observed in Figure 2 for the unit cell parameter variations.

One can also observe that the lowering of the crystallinity is significantly more pronounced for UiO-66(Zr) whatever the magnitude of the applied pressure. This trend is concomitant with a steeper decrease of the unit cell parameter for the non-functionalized solid (Figure 2). Typically, for an applied pressure of ~1.7 GPa, UiO-66(Zr) undergoes a slightly higher volume change ($\Delta V/V_0$=6.5%) compared to its amino functionalized form ($\Delta V/V_0$=4.3%) (See ESI). The incorporation of the amino function on the organic linker does not lead to a drastic change of the crystal density and porosity (free volume and theoretical accessible surface area-see Table 1). However, the $-NH_2$ groups introduce a steric hindrance (van der Waals volume of 90.4 $Å^3$ and 93.8 $Å^3$ for C_6H_6 and C_6H_5-NH_2 respectively). into the pore and allow establishing intra-framework interactions by the formation of hydrogen bonds between one of its hydrogen atom and the oxygen of the carboxylate group as previously shown by our DFT calculations (see Figure S14). [47] Both factors contribute to rigidify the framework leading to a lowering of the unit cell volume variation upon mechanical stimulus.

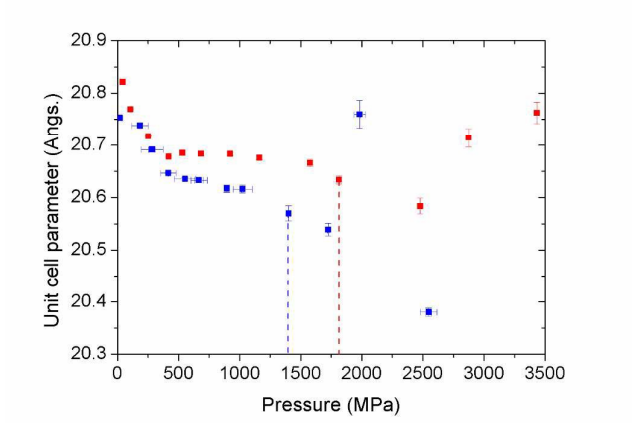

Fig. 2 *Evolution of the unit cell parameter a as a function of the applied pressure for UiO-66(Zr) (blue) and UiO-66(Zr)_NH_2) (red).*

To confirm this, the bulk modulus (K) for the two solids was estimated from the dependence of the unit cell volumes as a function of the pressure by applying the following equation $K = V_0\left(\frac{\partial P}{\partial V}\right)$ in the pressure range 0-1.5 GPa (See ESI Fig. S10 and S11). The so-obtained K value for UiO_66(Zr)_NH_2 (25(2) GPa) is significantly higher than that obtained for the non-functionalized solid (17(1.5) GPa) (Table S1). This observation confirms that the functionalization leads to a higher mechanical resilience of the solid, consistent with a lower magnitude of volume change and a lower loss of crystallinity. The so-obtained experimental bulk modulus for UiO-66(Zr), although significantly lower than the predicted value previously reported by DFT calculations (41 GPa), [19] is among the highest values reported so far for MOFs (see Table S2). This clearly emphasizes that this family of Zirconium based-MOFs above its exceptional thermal and chemical stabilities shows a high mechanical robustness.

To check whether the structural change of both solids is reversible or not, the XRPD patterns were collected once the applied pressure was released starting from the highest investigated pressure at 3.5 GPa. One observes that the corresponding data reported in Figure S4 and S5 perfectly match the PXRD patterns obtained for the pristine solid in terms of Bragg peak positions and widths. This clearly emphasizes the reversible nature of the structural modification.

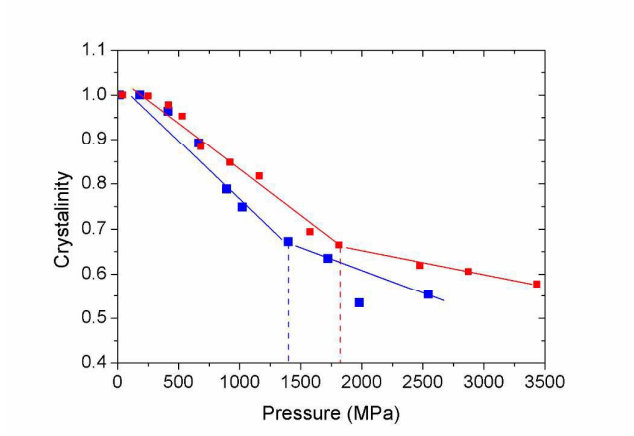

Fig. 3 *Evolution of the crystallinity for the (111) Bragg peak as a function of the applied pressure for UiO-66(Zr) (blue) and UiO-66(Zr)_NH_2) (red).*

Interestingly, Figure 3 shows that while the unit cell parameters for UiO-66(Zr) still decrease at the highest applied pressure, the scenario differs for UiO-66(Zr)_NH_2 with an increase of the cell dimensions. Such an evolution is characteristic of the instability of the structure of porous solids as was previously observed by Greaves *et al*. [48] on zeolites.

Regarding MIL-125(Ti) and MIL-125(Ti)_NH_2, the corresponding PRXD patterns under applied pressure are disclosed in Figure 4. All the diffraction patterns were indexed in the space group I4/mmm (See ESI Fig. S6 and S7) revealing no pressure induced phase transition up to ~3.8 GPa. Figure 5 shows the evolution of the unit cell parameters for MIL-125(Ti)s as a function of the applied pressure. A broadening of the (200) and (002) diffractions peaks is detected during the compression corresponding however to a loss of crystallinity but much less marked than for the UiO-66(Zr)s (See ESI Fig. S8 and S9). Further, both solids show smaller unit cell parameters changes compared to the UiO-66(Zr)s as well as an extended domain of stability up to 1.5 GPa as revealed by the shift of the step-change at higher pressure. Moreover, one can notice that the functionalization of this solid only slightly affects its structural mechanical behaviour. As an illustration, the magnitude of the $\Delta V/V_0$ change at ~2 GPa is 1.5% and 2.3% for MIL-125(Ti) and MIL-125(Ti)_NH_2 respectively (see Fig. S12 and S13) and the domain of stability spans in the same range of pressure.

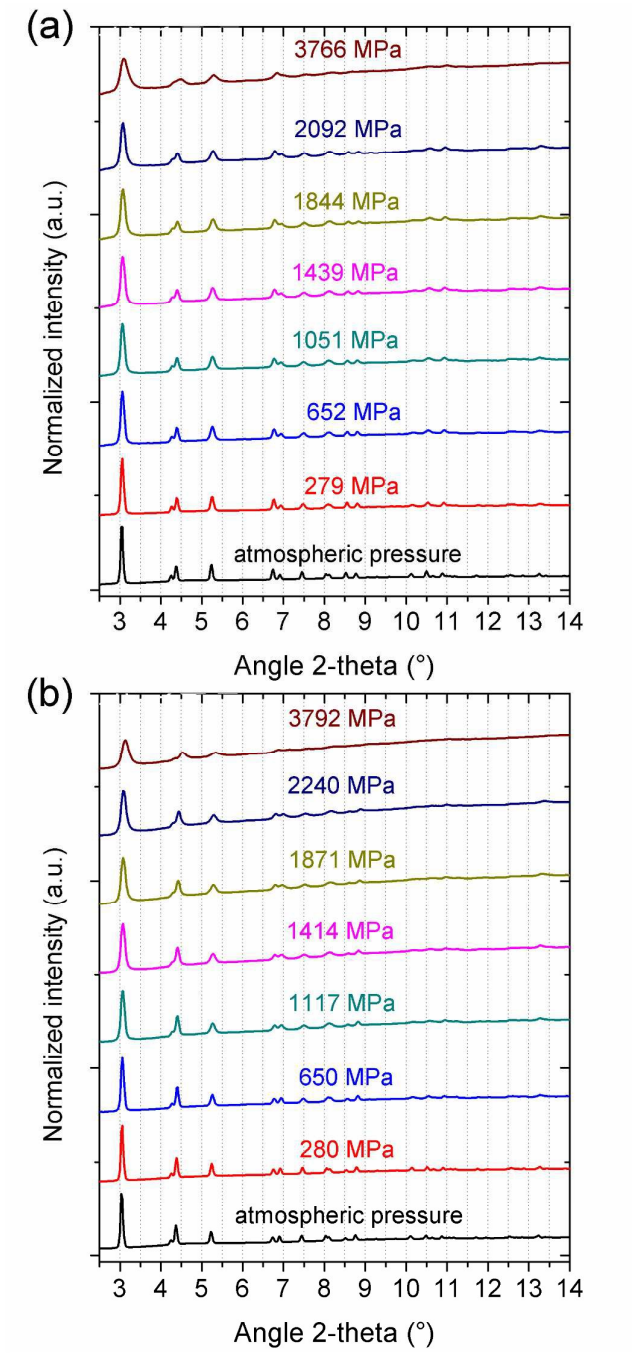

Fig. 4 *Powder X-ray diffraction patterns (λ= 0.694120 Å) obtained for the (a) MIL-125(Ti) and (b) MIL-125(Ti)_NH$_2$ as a function of the applied pressure at room temperature.*

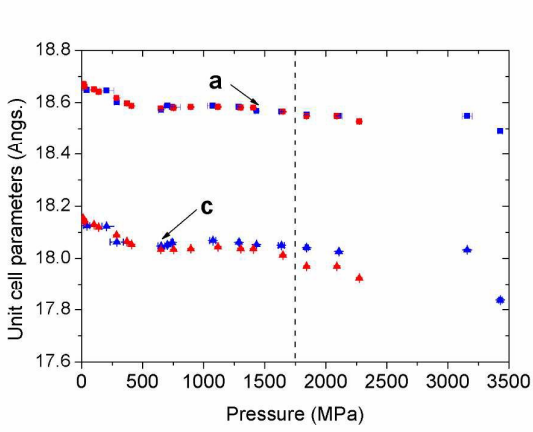

Fig. 5 *Evolution of the unit cell parameters as a function of the applied pressure for MIL-125(Ti) (blue) and MIL-125(Ti)_NH$_2$ (red).a parameter: square, c parameter: circle.*

The bulk modulus was estimated with the same method used for UiO-66(Zr)s. The resulting values are similar for both solids 10(2) GPa and 13(2) GPa for MIL-125(Ti) and MIL-125(Ti)_NH$_2$ respectively (See Table S1). The bulk moduli for MIL-125(Ti)s are thus significantly lower than the values obtained for UiO-66(Zr) analogues. This trend indicates that the mechanical resilience of a MOF solid decreases when the porosity increases and the crystal density decreases which supports what was evoked in a previous study dedicated to the investigation of the mechanical properties of a series of MOF-5 analogues (Table S3). [32] In addition, the higher compressibility of MIL-125(Ti)_NH$_2$ can be also related to a lowering of the metal-oxygen coordination (6 vs 8 for UiO-66(Zr)_NH$_2$).

Table 1 *Diameters of the octahedral/tetrahedral cages, the crystal density, accessible surface area and pore volume calculated from the crystal structures for all the investigated MOFs.*

	UiO-66(Zr)	UiO-66(Zr)_NH2	MIL-125(Ti)	MIL-125(Ti)_NH$_2$
Diameter of the octahedral/tetrahedral cages (Å)	7.8/6.8	6.8/5.9	12/6	10.7/4.7
Density ρ_{cyrst} (g/cm^3)	1.2098	1.2642	0.8241	0.8683
V_{pore} (cm^3/g)	0.45	0.40	0.76	0.72
S_{acc} (m^2/g) [11, 16, 13]	1018	848	2140	1730

Conclusion

This experimental work evidenced that beyond a very good chemical and thermal stability, the UiO-66(Zr) material and its amino functionalized version show a high mechanical resilience associated with one of the highest bulk moduli among the family of porous hybrid solids reported so far. In addition, no amorphization was evidenced for these solids under applied pressures up to 2 GPa. Only a gradual loss of crystallinity was detected under applied pressure and was revealed to be fully reversible once the mechanical constraint released. More interestingly, the functionalization of this solid, which was shown to significantly enhance its separation/adsorption properties with respect to a series of strategic gases such as CO_2, N_2 and CH_4, [13] also enhances the mechanical stability with a significant increase of the bulk modulus. This trend was explained by the additional intra-framework interactions introduced by the amino group. Such an

observation might be even truer for the di-acidic functionalized materials that have been revealed as one of the most promising MOFs for CO_2 capture in post-combustion conditions. [49] The mechanical resilience is also of great importance when one envisages the use of such hybrid solids in the design of composite membranes with polymers. By considering the MIL-125(Ti)s characterized by a higher porosity and a lower density, our experimental approach revealed that the mechanical stability and the high porosity are two competing factors. This information is of interest to further design MOFs with not only appropriate adsorption/separation properties but also mechanical resilience, a crucial pre-requisite for industrial applications. Finally, a future work will consider the impact of the defects on the mechanical properties of UiO-66(Zr) by considering samples containing different concentration of missing linkers.

Acknowledgements

The authors want to thank the European Synchrotron Radiation Facility (Grenoble, France) for beam time. French National Agency for Research ANR "MODS" (ANR-12-BS10-0005) is also acknowledged for its financial supports. G.M. thanks Institut Universitaire de France for its support.

References

1 G. Férey, *Chem. Soc. Rev.*, 2008, **37**, 191.
2 Themed issues: metal-organic frameworks, a) Chem. Rev. 2012, 112, 673; b) *Chem. Soc. Rev.* 2014, **43**, 5415.
3 N. C. Burtch, H. Jasuja and K. S. Walton, *Chem. Rev.*, 2014, **114**, 10575.
4 J. Canivet, A. Fateeva, Y.M. Guo, B. Coasne and D. Farrusseng, *Chem. Soc. Rev.*, 2014, **43**, 5594.
5 J.C Tan, T. D. Bennett and A. K. Cheetham, *PNAS*, 2010, **107**, 9938.
6 J. C. Tan and A. K. Cheetham, *Chem. Soc. Rev.*, 2011, **40**, 1059.
6 J.C. Tan and A.K. Cheetham, *Chem. Soc. Rev.*, 2011, **40**, 1059.
7 W. Li, M R Probert, M. Kosa, T. D. Bennett, A. Thirumurugan, R. P Burwood, M. Parinello, J. A. K. Howard and A. K. Cheetham, *J. Am. Chem. Soc.* 2012, 134, 11940.
8 W. Li, M. S. R. N. Kiran, J. L. Manson, J. A. Schlueter, A. Thirumurugan, U. Ramamurty and A. K. Cheetham, *Chem. Comm.*, 2013, **49**, 4471.
9 W. Li, S. Henke and A. K. Cheetham, *Apl. Materials*, 2014, **12**, 123902.
10 J. H. Cavka, S. Jakobsen, U. Olsbye, N. Guillou, C. Lamberti, S. Bordiga and K. P. Lillerud, *J. Am. Chem. Soc.*, 2008, **130**, 13850.
11 M. Dan-Hardi, C. Serre, T. Frot, L. Rozes, G. Maurin, C. Sanchez and G. Férey, *J. Am. Chem. Soc.*, 2009, **131**, 10857.
12 V. Guillerm, S. Gross, C. Serre, T. Devic, M. Bauer and G. Férey, *Chem. Commun.*, 2010, **46**, 767.
13 Q. Yang, A. D. Wiersum, P. L. Llewellyn, V. Guillerm, C. Serre and G. Maurin, *Chem. Commun.*, 2011, **47**, 9603.
14 F. Vermoortele, B. Bueken, G. Le Bars, B. Van de Voorde, M. Vandichel, K. Houthoofd, A. Vimont, M. Daturi, M. Waroquier, V. Van Speybroeck, C. Kirschhock and D. E. De Vos, *J. Am. Chem Soc.*, 2013, **135**, 11465.
15 J. Ye and J. Karl Johnson, *ACS Catal.*, 2015, **5**, 2921.
16 S. Vaesen, V. Guillerm, Q. Yang, A. D. Wiersum, B. Marszalek, B. Gil, A. Vimont, M. Daturi, T. Devic, P. L. Llewellyn, C. Serre, G. Maurin and G. De Weireld, *Chem. Commun.*, 2013, **49**, 10082.
17 T. Devic, C. Serre, *Chem Soc Rev.*, 2014, **43**, 6097.
18 V. Guillerm, F. Ragon, M. Dan-Hardi, T. Devic, M. Vishnuvarthan, B. Campo, A. Vimont, G. Clet, Q. Yang, G. Maurin, G. Férey, A. Vittadini, S. Gross and Christian Serre, *Angew. Chem. Int. Ed.*, 2012, **51**, 9267.
19 H. Wu, T. Yildirim and W. Zhou, *J. Phys. Chem. Lett.*, 2013, **4**, 925.
20 J. Hafizovic Cavka, S. Jakobsen, U. Olsbye, N. Guillou, C. Lamberti, S. Bordiga and K. P. Lillerud, *J. Am. Chem. Soc.*, 2008, **130**, 13850.
21 M. Kandiah, M. H. Nilsen, S. Usseglio, S. Jakobsen, U. Olsbye, M. Tilset, C. Larabi, E. A. Quadrelli, F. Bonino and K. P. Lillerud, *Chem. Mater.*, 2010, **22**, 6632.
22 M. A. Moreira, J. C. Santos, A. F. P. Ferreira, J. M. Loureiro, F. Ragon, P. Horcajada, P. G. Yot, C. Serre and A. E. Rodrigues, *Langmuir*, 2012, **28**, 3494.
23 G. C. Shearer, S. Chavan, J. Ethiraj, J. G. Vitillo, S. Svelle, U. Olsbye, C. Lamberti, S. Bordiga and K. P. Lillerud, *Chem. Mater.*, 2014, **26**, 4068–4071.
24 L.-M. Yang, E. Ganz, S. Svellec and M. Tilset, *J. Mater. Chem. C*, 2014, **2**, 7111-7125.
25 Z. Fang, B. Bueken, D. E. De Vos and Roland A. Fischer, *Angew. Chem. Int. Ed.*, 2015, **54**, 7234.
26 M. Vandichel, J. Hajek, F. Vermoortele, M. Waroquier, D. E. De Vos and V. Van Speybroeck, *Cryst. Eng. Comm.*, 2015, **17**, 395-406.
27 C. A. Trickett, K. J. Gagnon, S. Lee, F. Gandara, H.-B. Bîrgi and O. M. Yaghi, *Angew. Chem. Int. Ed.*, 2015, **54**, 11162.
28 K. W. Chapman, G. J. Halder, P. J. Chupas, *J. Am. Chem. Soc.*, 2008, **130**, 10524.
29 K. W. Chapman, G. J. Halder and P. J. Chupas, *J. Am. Chem. Soc.*, 2009, **131**, 17546.
30 T. D. Bennett, J. C. Tan, S. A. Moggach, R. Galvelis, C. Mellot-Draznieks, B. A. Reisner, A. Thirumurugan, D. R. Allan, A. K. Cheetham, *Chem. Eur. J.*, 2010, **16**, 10684.
31 T. D. Bennett, P. Simoncic, S. A. Moggach, F. Gozzo, P. Macchi, D. A. Keen, J.-C. Tan and A. K. Cheetham, *Chem. Commun.*, 2011, **47**, 7983.
32 A. J. Graham, D. R. Allan, A. Muszkiewicz, C. A. Morrison, and S. A. Moggach, *Angew. Chem. Int. Ed.*, 2011, **50**, 11138.
33 A. Ghoufi, A. Subercaze, Q. Ma, P. G. Yot, Y. Ke, I. Puente Orench, T. Devic, V. Guillerm, C. Zhong, C. Serre, G. Férey and G. Maurin, *J. Phys. Chem. C*, 2012, **116**, 13289.
34 P.G. Yot, Q. Ma, J. Haines, Q. Yang, A. Ghoufi, T. Devic, C. Serre, V. Dmitriev, G. Férey, C. Zhong and G. Maurin, *Chem. Sci.*, 2012, **3**, 1100.
35 S. A. Moggach, A. J. Graham, A. Muszkiewicz, C. A. Morrison, *Int. J. of Nanotechnology*, 2010, 9, 18.
36 J. M. Ogborn, I. E. Collings, S. A. Moggach, A. Stephen, A. L. Thompson and A. L. Goodwin, *Chem. Sci.*, 2012, **3**, 3011.
37 P. Serra-Crespo, E. Stavitski, F. Kapteijn and J. Gascon, *RSC Adv.*,2012, **2**, 5051.
38 T. D. Bennett, P. J. Saines, D. A. Keen, J. C. Tan and A. K. Cheetham, *Chem. – Eur. J.*, 2013, **19**, 7049.
39 A. J. Graham, A. M. Banu, T. Duren, A. Greenaway, S. C. McKellar, J. P. S. Mowat, K. Ward, P. A. Wright and S. A. Moggach , *J. Am. Chem. Soc.*, 2014, **136**, 17546.
40 E. C. Spencer, M. S. R. N. Kiran, W. Li, U. Ramamurty, N. L. Ross and A. K. Cheetham, *Angew. Chem. Int. Ed.*, 2014, **53**, 5583-5586.

41 P. G. Yot, Z. Boudene, J. Macia, D. Granier, L. Vanduyfhuys, T. Verstraelen, V. Van Speybroeck, T. Devic C. Serre, G. Férey, N. Stock and G. Maurin, *Chem. Comm.*, 2014, **50**, 9462.
42 T. D. Bennett, J. Sotelo, J.-C. Tan and S. A. Moggach, *CrystEngComm*, 2015, **17**, 286.
43 B. Van de Voorde, I. Stassen, B. Bueken, F. Vermoortele, D. De Vos, R. Ameloot, J.-C. Tan and T. D. Bennett, *J. Mater. Chem. A*, 2015, **3**, 1737.
44 P. G. Yot, L. Vanduyfhuys, E. Alvarez, J. Rodriguez, J.-P. Itié, P. Fabry, N. Guillou, T. Devic, I. Beurroies, P. L. Llewellyn, V. Van Speybroeck, C. Serre and G. Maurin, *Chem. Sci.*, 2015 DOI: 10.1039/c5sc02794b.
45 V. Petricek, M. Dusek and L. Palatinus, *Z. Kristallogr.*, 2014, **229**, 345.
47 S. Devautour-Vinot, G. Maurin, C. Serre, P. Horcajada, D. Paula da Cunha†, V. Guillerm†, E. de Souza Costa, F. Taulelle and C. Martineau, *Chem. Mater.*, 2012, **24**, 2168.
48 G. N. Greaves, F. Meneau, A. Sapelkin, L. M. Colyer, I. ap Gwynn, S. Wade and G. Sankar, *Nature Materials*, 2003, **2**, 622.
49 Q. Y. Yang, S. Vaesen, F. Ragon, A. D. Wiersum, D. Wu, A. Lago, T. Devic, C. Martineau, F. Taulelle, P.L. Llewellyn, H. Jobic, C. L. Zhong, C. Serre, G. De Weireld and G. Maurin, *Angew. Chem. Int. Ed.*, 2013, **52**, 10316.

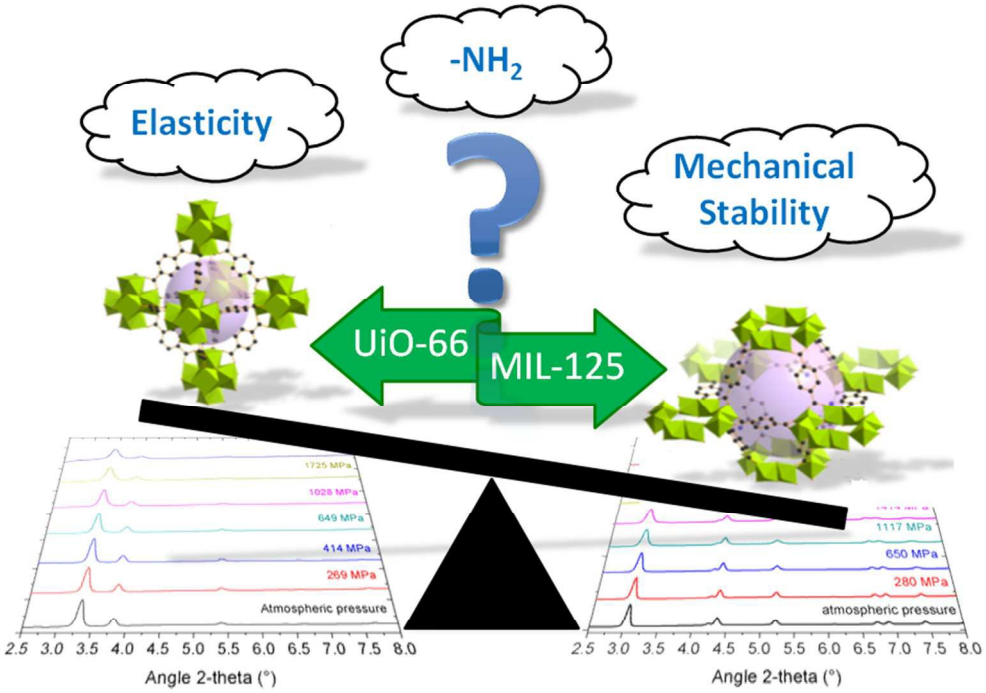

254x190mm (96 x 96 DPI)